Optical-vortex laser ablation

Junichi Hamazaki[1,*], Ryuji Morita[1], Keisuke Chujo[2], Yusuke Kobayashi[2], Satoshi Tanda[1], and Takashige Omatsu[2]

[1] *Department of Applied Physics, Hokkaido University, Sapporo, 060-8628, Japan*
[2] *Graduate School of Advanced Integration Science, Chiba University, Chiba, 263-5822, Japan*
* *hamazaki@topology.coe.hokudai.ac.jp*

Abstract: Laser ablation of Ta plates using nanosecond optical vortex pulses was carried out, for the first time. It was suggested that owing to orbital angular momentum of optical vortex, clearer and smoother processed surfaces were obtained with less ablation threshold fluence, in comparison with the ablation by a nonvortex annular beam modified from a spatially Gaussian beam.

OCIS codes: (140.3390) Laser materials processing; (140.3300) Laser beam shaping; (999.9999) Optical vortices;

References and links

1. D. Bäuerle, *Laser processing and chemistry*, 3rd ed., (Springer-Verlag, Berlin, Heidelberg 2000).
2. J. C. Miller, and R. F. Haglund, *Laser ablation and desorption*, (San Diego, Academic Press, 1998).
3. M. C. Gower, "Industrial applications of laser micromachining," Opt. Express **7**(2), 56–67 (2000).
4. P. R. Willmott, and J. R. Huber, "Pulsed laser vaporization and deposition," Rev. Mod. Phys. **72**(1), 315–328 (2000).
5. S. Preuss, A. Demchuk, and M. Stuke, "Sub-picosecond UV laser ablation of metals," Appl. Phys., A Mater. Sci. Process. **61**(1), 33–37 (1995).
6. R. Le Harzic, D. Breitling, M. Weikert, S. Sommer, C. Föhl, F. Dausinger, S. Valette, C. Donnet, and E. Audouard, "Ablation comparison with low and high energy densities for Cu and Al with ultra-short laser pulses," Appl. Phys., A Mater. Sci. Process. **80**, 1589–1593 (2005).
7. A. Weck, T. H. R. Crawford, D. S. Wilkinson, H. K. Haugen, and J. S. Preston, "Laser drilling of high aspect ratio holes in copper with femtosecond, picosecond and nanosecond pulses," Appl. Phys., A Mater. Sci. Process. **90**(3), 537–543 (2008).
8. S. Paul, S. I. Kudryashov, K. Lyon, and S. D. Allen, "Nanosecond-laser plasma-assisted ultradeep microdrilling of optically opaque and transparent solids," J. Appl. Phys. **101**, 043106–1–8 (2007).
9. N. M. Bulgakova, and A. V. Bulgakov, "Pulsed laser ablation of solids: transition from normal vaporization to phase explosion," Appl. Phys., A Mater. Sci. Process. **73**(2), 199–208 (2001).
10. C. Körner, R. Mayerhofer, M. Hartmann, and H. W. Bergmann, "Physical and material aspects in using visible laser pulses of nanosecond duration for ablation," Appl. Phys., A Mater. Sci. Process. **63**(2), 123–131 (1996).
11. X. Zeng, X. L. Mao, R. Greif, and R. E. Russo, "Experimental investigation of ablation efficiency and plasma expansion during femtosecond and nanosecond laser ablation of silicon," Appl. Phys., A Mater. Sci. Process. **80**(2), 237–241 (2005).
12. N. Zhang, X. Zhu, J. Yang, X. Wang, and M. Wang, "Time-resolved shadowgraphs of material ejection in intense femtosecond laser ablation of aluminum," Phys. Rev. Lett. **99**(16), 167602 (2007).
13. L. Allen, M. W. Beijersbergen, R. J. C. Spreeuw, and J. P. Woerdman, "Orbital angular momentum of light and the transformation of Laguerre-Gaussian laser modes," Phys. Rev. A **45**(11), 8185–8189 (1992).
14. M. Padgett, J. Courtial, and L. Allen, "Light's orbital angular momentum," Phys. Today **57**(5), 35–40 (2004).
15. M. S. Soskin, and M. V. Vasnetsov, "Optical vortices," in Progress in Optics, Vol. 42, E. Wolf, ed., (Elsevier, North-Holland, 2001).
16. M. J. Padgett, and L. Allen, "The Poynting vector in Laguerre-Gaussian laser modes," Opt. Commun. **121**(1-3), 36–40 (1995).
17. J. Hamazaki, Y. Mineta, K. Oka, and R. Morita, "Direct observation of Gouy phase shift in a propagating optical vortex," Opt. Express **14**(18), 8382–8392 (2006).
18. J. Arlt, "Handedness and azimuthal energy flow of optical vortex beams," J. Mod. Opt. **50**, 1573–1580 (2003).
19. T. Kuga, Y. Torii, N. Shiokawa, T. Hirano, Y. Shimizu, and H. Sasada, "Novel optical trap of atoms with a doughnut beam," Phys. Rev. Lett. **78**(25), 4713–4716 (1997).
20. K. T. Gahagan, and G. A. Swartzlander, Jr., "Optical vortex trapping of particles," Opt. Lett. **21**(11), 827–829 (1996).
21. L. Paterson, M. P. MacDonald, J. Arlt, W. Sibbett, P. E. Bryant, and K. Dholakia, "Controlled rotation of optically trapped microscopic particles," Science **292**(5518), 912–914 (2001).

#120076 - $15.00 USD Received 16 Nov 2009; revised 20 Dec 2009; accepted 7 Jan 2010; published 19 Jan 2010

22. A. Mair, A. Vaziri, G. Weihs, and A. Zeilinger, "Entanglement of the orbital angular momentum states of photons," Nature **412**(6844), 313–316 (2001).
23. F. Caridi, L. Torrisi, D. Margarone, A. Picciotto, A. M. Mezzasalma, and S. Gammino, "Energy distributions of particles ejected from laser generated pulsed plasmas," F. Czech. J. Phys. **56**(S2), B449–B456 (2006).
24. L. Torrisi, F. Caridi, A. Picciotto, D. Margarone, and A. Borrielli, "Particle emission from tantalum plasma produced by 532 nm laser pulse ablation," J. Appl. Phys. **100**(9), 093306 (2006).
25. L. Torrisi, G. Ciavola, S. Gammino, L. Andò, A. Barnà, L. Láska, and J. Krása, "Metallic etching by high power Nd:yttrium-aluminum-garnet pulsed laser irradiation," Rev. Sci. Instrum. **71**(11), 4330–4334 (2000).
26. M. W. Beijersbergen, R. P. C. Coerwinkel, M. Kristensen, and J. P. Woerdman, "Helical-wavefront laser beams produced with a spiral phase plate," Opt. Commun. **112**(5-6), 321–327 (1994).
27. V. G. Niziev, and A. V. Nesterov, "Influence of beam polarization on laser cutting efficiency," J. Phys. D **32**(13), 1455–1461 (1999).
28. G. D. M. Jeffries, J. S. Edgar, Y. Zhao, J. P. Shelby, C. Fong, and D. T. Chiu, "Using polarization-shaped optical vortex traps for single-cell nanosurgery," Nano Lett. **7**(2), 415–420 (2007).
29. N. Bokor, Y. Iketaki, T. Watanabe, and M. Fujii, "Investigation of polarization effects for high-numerical-aperture first-order Laguerre-Gaussian beams by 2D scanning with a single fluorescent microbead," Opt. Express **13**(26), 10440–10447 (2005).
30. K. Venkatakrishnan, and B. Tan, "Interconnect microvia drilling with a radially polarized laser beam," J. Micromech. Microeng. **16**(12), 2603–2607 (2006).
31. S. Paul, S. I. Kudryashov, K. Lyon, and S. D. Allen, "Nanosecond-laser plasma-assisted ultradeep microdrilling of optically opaque and transparent solids," J. Appl. Phys. **101**(4), 043106 (2007).

1. Introduction

The laser ablation technique is one of the most promising methods for material processing. Since 1960's, laser ablation processing has been developed, together with evolution of light sources [1–4]. For industrial applications, high processing accuracy and low cost are required. These requirements have motivated a lot of researches of laser ablation, mainly in terms of morphology of processed surface and drilling efficiency, and their pulse energy or duration dependences [5–9]. Laser ablation dynamics using nanosecond (ns)-pulse in nontransparent materials was interpreted so far, as follows [1,2,9–12]: (i) Energy of absorbed light is first transferred to the electron system, and then to the lattice system owing to electron-phonon interaction. (ii) Lattice reaches equilibrium through phonon-phonon interaction and its temperature increases. (iii) High-temperature-induced phase transition occurs from solid state to liquid, gaseous, and plasma states. (iv) A pressure or a shock wave separates from the dense, hot focal volume, together with plasma plume expansion at high velocity (plasma expulsion).

In 1990's, generation of an optical vortex (OV) was demonstrated [13]. Since OVs have orbital angular momentum (OAM) of light owing to a phase distribution of $m\varphi$ (m; integer, called topological charge, φ; azimuthal angle) in transverse plane, OVs have been intensively investigated and attracted much attention [14,15]. Regarded as a new parameter of light, OAM has recently begun to be employed in various experiments, for example, information using multidimensional entangled states, especially trapping for Bose-Einstein condensates (BECs), microstructure rotation in laser tweezers and spanners etc [16–22]. In particular, in optical tweezing, OVs are used because they can trap and manipulate particles with less intensity than Gaussian beam (GB), which results in less absorption or photodamage due to multiphoton processes. In addition, more efficient tweezing can be achieved thanks to the loss of the rays in the center of the beam. Analogously, efficient ablation may be expected with OVs. However, OVs have not been used in laser ablation and not studied their OAM effect on the ablation processes and results.

In the present paper, we demonstrate the laser ablation using ns-optical vortex pulses. We show that the ablation with OVs yields smoother processed surfaces and deeper drilling than that with the reference pulse, which has a modified Gaussian spatial profile with a center hole. Moreover, we suggest an explanation of OAM effects on the laser ablation processes. Our demonstration represents a novel and better laser ablation technique using OV pulses and our model provides another key to applications of laser plasma employing OVs.

#120076 - $15.00 USD Received 16 Nov 2009; revised 20 Dec 2009; accepted 7 Jan 2010; published 19 Jan 2010

2. Experiments

2.1 Experimental setup

Figure 1(a) shows a schematic drawing of an experimental setup for ns-laser ablation system using OV pulses. The experiments were performed in atmospheric pressure and at room temperature. Tantalum (Ta) plates were used as target samples. They exhibit low ablation threshold in comparison with other metals [23–25], which enables us to perform ablation experiment easily. Thickness of the Ta plates was ~1 mm and the plate surfaces were polished by sandpaper. As a light source, we used a conventional Q-switched ns-Nd:YAG laser (Quanta-Ray GCR190) generating a spatially fundamental GB (HG_{00}) with a wavelength of 1064 nm and a pulse duration of ~40 ns. This laser can be operated in a single-shot mode. A spiral phase plate (SPP) modulating spatial phase azimuthally (custom-made) was used to produce OVs [26]. A combination of a telescope and a spatial filter (SF) containing 3-mm-diameter aperture was employed to improve spatial beam profiles. Figures 1(b) and 1(c) show intensity patterns of OV (m = 2) and OV (m = 1) on the sample surface, respectively. A typical self-shearing interference profile of the OV beam (m = 2) observed in a Mach-Zehnder interferometer is shown in Fig. 1(d). Two-fork pattern is clearly seen, indicating on-axis phase singularity of the beam.

To make a clear difference between ablation results with and without OAM effects, we used a *nonvortex annular beam* (NVAB) modified from a spatially GB as a reference incidence. NVAB was generated from a 3-mm-diameter GB by passing through a spatial notch filter (SNF) which blocks 1-mm-diameter region at the beam center, as shown in Fig. 1(e). Therefore, NVAB has no OAM (m = 0). NVAB also has doughnut-like intensity profile on the sample surface similar to the OV profiles as shown in Fig. 1(f). The intensity line profiles for NVAB and OV with m = 2 are quite similar even in the beam edges, as shown in Fig. 1(g).

Using a convex lens (L) with a focal length of 50 mm, the OVs and NVAB were roughly focused. All the focal positions were at the same position. Sample surfaces were slightly located off the focal planes (~2 mm away), where the beam spot sizes were ~130 μm. On the sample surfaces, the center dark spots were kept even for NVAB (Since NVAB is not an eigen-solution of the paraxial equation, the dark spot at the center of NVAB disappears in the focal plane). Incident pulse energy was varied in the range of 0.3-3 mJ. After a single-shot-pulse laser ablation, ablated surfaces of Ta plates were observed under a confocal laser-scanning microscope (VK-9700/VK9710GS, Keyence Corp.), which measures depth as a function of transverse position with an accuracy of ~0.02 μm in depth and a resolution of ~0.02 μm in transverse displacement.

2.2 Experimental results

Figures 2(a)-2(c) show typical morphology of processed surfaces for (a) the OV (m = 2) and (b) OV (m = 1) pulses with incident pulse energy of 3 mJ, together with (c) NVAB as a reference. The processed surface for NVAB (Fig. 2(c)) was rough and a lot of debris were seen in the radial direction around the outer circumference. In good contrast to this, for the OV with m = 2 (Fig. 2(a)), smoother-processed surface was observed and numbers of debris were significantly reduced in comparison with the case of NVAB. The processed surface for the OV with m = 1 (Fig. 2(b)) showed an intermediate tendency between those for the OV with m = 2 and NVAB.

#120076 - $15.00 USD Received 16 Nov 2009; revised 20 Dec 2009; accepted 7 Jan 2010; published 19 Jan 2010

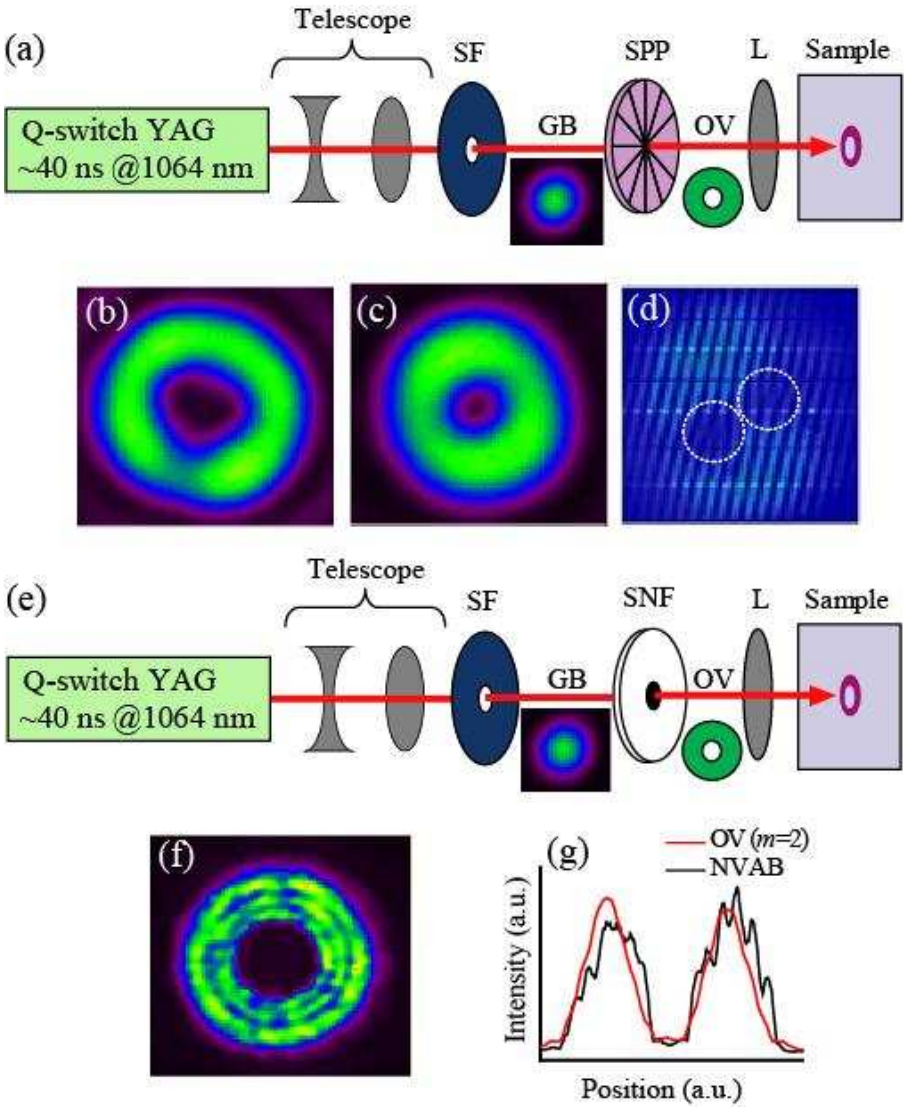

Fig. 1. (a) Experimental setup of laser ablation using OVs. SF is a spatial filter, SPP is a phase plate to generate OVs, L is a convex lens with a focal length of 50 mm. Intensity profile of GB is shown. (b) Intensity profiles of the OV (m = 2), (c) OV (m = 1) on the sample surface. (d) Shearing interference pattern of OV (m = 1) in the Mach-Zehnder configuration. Dotted-circles indicate phase singularities. (e) Experimental setup of laser ablation using NVAB. SNF is spatial notch filter. (f) Intensity profiles of NVAB on the sample surface. (g) Horizontal intensity profiles of the OV (m = 2) and NVAB.

For high-numerical aperture (NA) configuration with NA~1, the beam polarization dependences of ablation results as well as intensity profiles have been reported [27–30]. In ref [27], it was pointed out that these polarization dependences were due to the effects of angles between electric-field vectors and processed surfaces, which govern the absorption efficiency at processed surfaces. In contrast, in the present experiment where we employed a low NA configuration (NA~0.03), beam polarization dependence may be small. Therefore, with only linearly polarized beams, we performed the experiment to investigate OAM effects on ablation results. Note that while incident beams were polarized in a horizontal direction, angle dependences in processed surface morphology were not observed.

#120076 - $15.00 USD Received 16 Nov 2009; revised 20 Dec 2009; accepted 7 Jan 2010; published 19 Jan 2010

Figures 3(a)-3(c) show distributions of the second-order derivative of the relative height of processed surfaces with respect to the radial coordinate, indicating the surface curvature given by $\partial^2 h(r,\theta)/\partial r^2$, where h, r and θ denote relative height, radius and azimuthal angle in the 2-dimensional polar coordinates, respectively. The relative height is measured from the height of non-processed surface. The origin of the polar coordinates is set to be the center position of the processed surface, corresponding to the center of the incident beam. Generally, the surfaces are drilled by the laser ablation process and some portion of the ablated material is piled up outside (or around the vicinity of the center), as shown in Fig. 3(d). Therefore, the values of $\partial^2 h(r,\theta)/\partial r^2$ become positive and negative inside and outside of the ablated region, respectively [26]. Thus, its sign change gives the measure of clearness of the outline for ablated region. In the cases of OVs with m = 2 and 1 (Fig. 3(a) and 3(b)), the outline structures were much clearer than that for NVAB (Fig. 3(c)). Moreover, the processed surface for OV with m = 2 was smoother than that for OV with m = 1, implying that the larger topological charge induces the clearer outline structure on the processed surface.

Features of processed surface roughness are obtained by spatial Fourier analysis. A normalized spectrum of the relative height h for the processed surface directly shows the amount of undulation in a certain spatial frequency or a certain period, as illustrated in Figs. 4(a)-4(d). Here, since areas of processed surfaces for OVs and NVAB are same, the normalization was done with dividing amplitudes by average heights. For example, the spatial Fourier spectra for near ideal ablation results show small Fourier-amplitude in the whole spatial-frequency region except near zero-spatial-frequency.

Figure 5(a) shows the normalized spatial frequency spectra of r-averaged relative height $h_1(\theta)$ for the ablation results by OV and NVAB, together with that by a GB. Figure 5(b) shows the normalized spatial frequency spectra of θ-averaged relative height $h_2(r)$ in the similar ma-

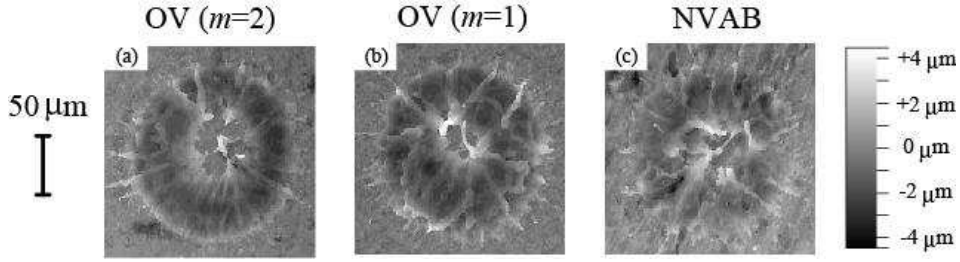

Fig. 2. Laser microscope images of processed surfaces for (a) the OV with m = 2 (b) OV with m = 1, and (c) NVAB with incident energy of 3 mJ/pulse, respectively. Dotted circles denote debris.

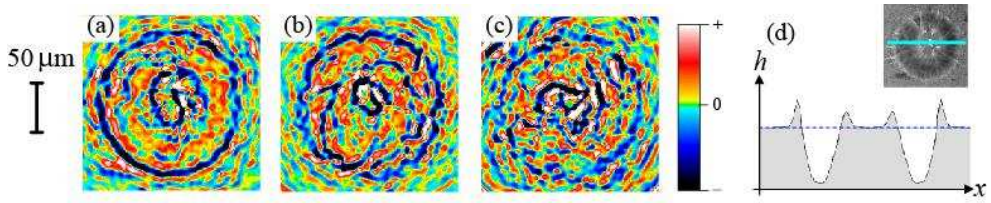

Fig. 3. Curvature distribution of the relative height h in radial direction for (a) OV with m = 2, (b) OV with m = 1, and (c) NVAB. (d) Cross-section illustration of processed surface along the blue line (x-axis) in the inset of figure.

#120076 - $15.00 USD Received 16 Nov 2009; revised 20 Dec 2009; accepted 7 Jan 2010; published 19 Jan 2010

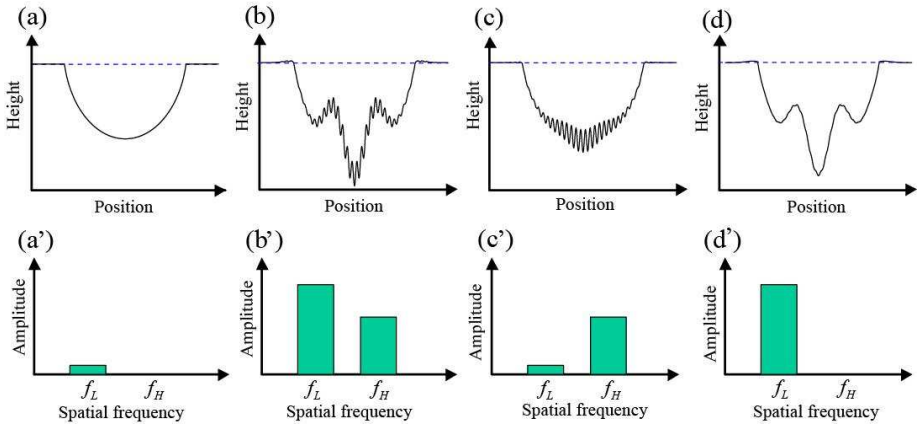

Fig. 4. Schematic cross-section of ablated zone with (a) smooth surface, (b) rough surface with low- and high-spatial-frequency undulations, (c) rough surface with high-spatial-frequency undulation, and (d) rough surface with low-spatial-frequency undulation. (a')-(d') Corresponding schematic of spatial Fourier distributions for (a)-(d), respectively. Amplitudes at zero-spatial-frequency are excluded.

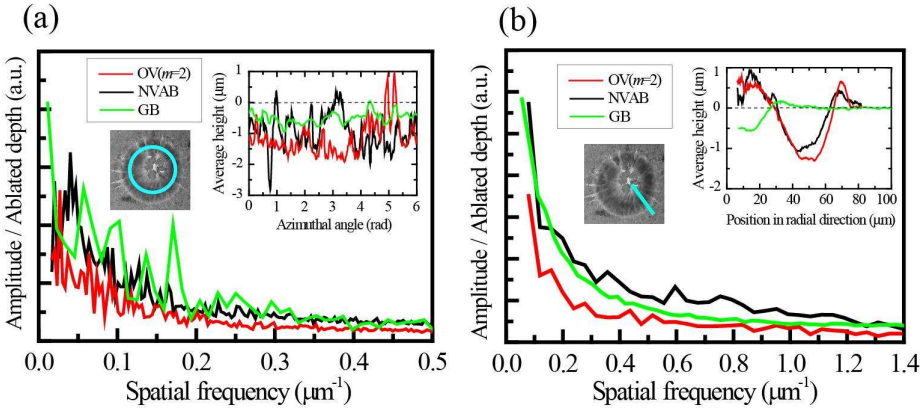

Fig. 5. Spatial Fourier spectra for (a) r- and (b) θ-averaged height profiles. Insets of (a) and (b) show r- and θ-averaged height distributions which are along pathways shown by blue lines in the inset images. Red, black, and green lines are spatial frequency spectra and height distributions for OV with $m = 2$, for NVAB, and GB, respectively.

-nner. Insets of Figs. 5(a) and 5(b) show relative height distributions $h_1(\theta)$ and $h_2(r)$ in the azimuthal and radial directions, respectively, of which pathways were shown in the corresponding images. In the azimuthal direction (Fig. 5(a)), it is clear that the amplitude for the OV with $m = 2$ is smaller than those for NVAB and GB in the whole spatial-frequency region. This indicates that the processed surface in azimuthal direction for OV with $m = 2$ was smoother than those for NVAB and GB. In the radial direction (Fig. 5(b)), the amplitude for the OV with $m = 2$ is smaller than those for NVAB and GB, in the whole spatial frequency region. This manifests that undulations with any spatial in radical direction for the OV with $m = 2$ were less than those corresponding to NVAB and GB. Thus, it is clearly evaluated that the processed surface for the OV with $m = 2$ was smoother than those for NVAB and GB.

Figure 6 shows ablated depth D as a function of incident fluence F, for OV with $m = 2$ and NVAB. The depth D was evaluated as an absolute value of the minimum of $h_2(r)$ (see Fig. 3(d)). At any fluence, the ablated depth for the OV with $m = 2$ was deeper than that for NVAB. It is known the ablation depth dependence was described by a logarithmic low

#120076 - $15.00 USD Received 16 Nov 2009; revised 20 Dec 2009; accepted 7 Jan 2010; published 19 Jan 2010

as $D = \xi \ln(F/F_{th})$, where ξ and F_{th} denote optical penetration depth and ablation-threshold fluence, respectively [5,12]. Using this expression, the ablation-threshold fluence was evaluated to be about 1.5 J/cm^2 and 3.3 J/cm^2 for the OV with m = 2 and NVAB, respectively, on the assumption of same values in optical penetration depth ξ for both cases. This is a reasonable assumption since the optical penetration depth was determined by material parameters and incident wavelength [25].

3. Discussion

Our experimental results as described in the previous section are summarized as follows: 1) The processed surfaces by OVs are clearer and smoother, having less debris, than that by NVAB. 2) The ablation-threshold fluence with OVs is less than that with NVAB. We discuss here the differences between ablation results with OVs and NVAB.

In the present experiments, while NVAB and OVs are both horizontally-polarized and have doughnut-beam intensity profiles with the similar-edge steepness (see Fig. 1(g)), they gave the different ablation results. It is considered that the differences between ablation results with OVs and NVAB can be due to (i) the OAM effect or (ii) the slight difference in spatial profiles between OVs and NVAB. Spatial profiles of OVs and NVAB are quite similar but only the spatial profile of NVAB has slight ring-shaped undulation owing to diffraction, as shown in Fig. 1(f). This undulation may affect the smoothness of the processed surface. Concerning spatial intensity profile of NVAB, while r-averaged intensity profile $I_1(\theta)$ in the azimuthal direction was smoother, θ-averaged intensity profile $I_2(r)$ in the radial direction has an undulation with a characteristic period of ~10 μm. For averaged height profiles $h_1(\theta)$ and $h_2(r)$ in the corresponding processed surfaces, both amplitudes of their spatial Fourier spectra were greater than those for OVs in whole spatial-frequency region. These worse ablation results may be explained by the undulated intensity profile of NVAB, however, there was no characteristic spatial frequency in the Fourier spectra of $h_2(r)$ unlike that of $I_2(r)$. In addition, even spatial Fourier spectrum for $h_2(r)$ of the ablated surface by GB without any intensity undulation was greater than that by OV in whole spatial-frequency region, indicating that the ablated surface by GB was rougher than those by OVs. Moreover, ablated depth using OV with m = 2 was deeper than that using NVAB and the evaluated ablation threshold fluence for the OV with m = 2 was fairly less than that for NVAB. Theses quantitative differences may not be explained by considering only undulation in intensity profile of the beams. Hence, as an alternative explanation, we suggest that the differences between ablation results are mainly ascribed to the OAM effect.

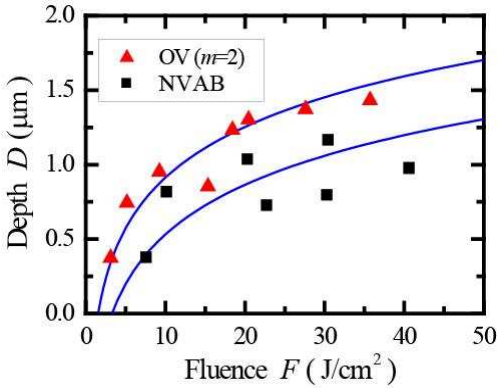

Fig. 6. Ablated depth D as a function of incident fluence F. Red triangles and black squares correspond to cases for OV with m = 2 and NVAB, respectively. Blue lines denote fitting curves using the expression of $D = \xi \ln(F/F_{th})$ (see the text).

#120076 - $15.00 USD Received 16 Nov 2009; revised 20 Dec 2009; accepted 7 Jan 2010; published 19 Jan 2010

The OAM effect is described as follows. In the analogue of optical tweezing or manipulation using OV, the OAM may cause the effects of rotational motion of molten material and/or laser-induced plasma through the OAM transfer by absorbing photons. The former is that rotational motion of molten material to which OAM is transferred from photons makes smoother processed surfaces. The latter is that rotational motion of laser-induced plasma to which OAM is transferred assists the ablation processes, leading to smoother surfaces. This is in an extension of the ablation assisted by laser-induced-plasmas, which was reported in ref [31]. We cannot yet mention that those effects are dominant in the present experiments. This will be discussed elsewhere with new experimental results.

4. Conclusion

We performed laser ablation of Ta plates using nanosecond OV pulses, for the first time, observing the morphology of the Ta surface after single-shot laser irradiation. We found that the laser ablation by an OV pulse yielded (i) clearer outline of the ablated zone, (ii) less debris, (iii) less ablation threshold fluence, and (iv) smoother processed surface, than that by NVAB modified from a HG_{00} beam. It was suggested that in comparison with ablation results by NVAB or GB, these improvements were attributed to the OAM effects.

Our demonstration using OV pulses represents a novel and better laser ablation technique, for example, in industries, fine, clear and smooth processing with less ablation threshold. In addition, it gives possibilities of annular ablation processing fabricating structures micro-pillar, pillar-based photonic crystals or meta-materials. Furthermore, our results provide another key to applications of laser plasma employing OVs, such as spatial confinement and control of plasmas.

Acknowledgment

This work was partially supported by Grant-in-Aid for the 21st Century COE program on "Topological Science and Technology" from the Ministry of Education, Culture, Sports, Science and Technology of Japan, and Grant-in-Aid for Scientific Research (B), 2008-2010, No. 20360025 from Japan Society for the Promotion of Science (JSPS).

#120076 - $15.00 USD Received 16 Nov 2009; revised 20 Dec 2009; accepted 7 Jan 2010; published 19 Jan 2010